Nonchiral edge states at the chiral metal-insulator transition in disordered quantum Hall wires

Alexander Struck,[1] Bernhard Kramer,[1] Tomi Ohtsuki,[1,2] and Stefan Kettemann[1]
[1]*I. Institut für Theoretische Physik, Universität Hamburg, Jungiusstraße 9, 20355 Hamburg, Germany*
[2]*Department of Physics, Sophia University, Kioi-Choi 7-1, Chiyoda-Ku, Tokyo 102-8554, Japan*
(Received 12 January 2005; revised manuscript received 13 May 2005; published 19 July 2005)

The quantum phase diagram of disordered wires in a strong magnetic field is studied as a function of wire width and energy. The two-terminal conductance shows zero-temperature discontinuous transitions between exactly integer plateau values and zero. In the vicinity of this transition, the chiral metal-insulator transition (CMIT), states are identified that are superpositions of edge states with opposite chirality. The bulk contribution of such states is found to decrease with increasing wire width. Based on exact diagonalization results for the eigenstates and their participation ratios, we conclude that these states are characteristic for the CMIT, have the appearance of nonchiral edges states, and are thereby distinguishable from other states in the quantum Hall wire, namely, extended edge states, two-dimensionally (2D) localized, quasi-1D localized, and 2D critical states.

DOI: 10.1103/PhysRevB.72.035339 PACS number(s): 72.10.Fk, 72.15.Rn, 73.20.Fz

I. INTRODUCTION

Recently, there has been renewed interest in quantum Hall bars of finite width, where the interplay between localized states in the bulk of the two-dimensional electron system (2DES) and edge states with energies lifted by the confinement potential above the energies of centers of bulk Landau bands, E_{n0},[1] results in the quantization of the Hall conductance. The study of mesoscopically narrow quantum Hall bars[2] revealed additional types of conductance fluctuations,[3,4] edge state mixing,[5–7,9,23] the breakdown of the quantum Hall effect,[10] and the quenching of the Hall effect due to classical commensurability effects.[11] In the presence of white noise disorder the edge states do mix with the bulk states when the Fermi energy is moved into the center of a Landau band. It had been suggested that this might result in localization of edge states.[7–9] Recently, it has been shown that at zero temperature the two-terminal conductance of a quantum wire in a magnetic field exhibits for uncorrelated disorder and hard wall confinement discontinuous transitions between integer plateau values and zero.[12] These transitions have been argued to be due to sharp localization transitions of chiral edge states, where the localization length of the edge states jumps from *exponentially large* to finite values, driven by the dimensional crossover of localized bulk states, and are accordingly called chiral metal-insulator transitions (CMIT's).

In this article, we will study the nature of this transition in more detail, and in particular find that at this transition there exists a type of state with properties distinguishable from both localized and extended bulk states, and extended edge states. This state is a superposition of edge states with opposite chirality. Since it is still located mainly close to the edges, we will call this state a *nonchiral edge state*.

The article is organized in the following way. In the next section, we present transfer matrix calculations of the quantum phase diagram of a quantum Hall bar with uncorrelated disorder, being characterized by the two-terminal conductance G as a function of energy E and width w of the wire. Sharp jumps in the conductance from integer values to zero are found as a function of energy. These CMIT's are seen to become more pronounced with increasing wire widths w.

In the third section we will study with exact diagonalization the eigenstates of a disordered quantum Hall wire. We will classify these states into five classes, the edge states, the 2D localized states, the quasi-1D localized states, the 2D extended states, and the nonchiral edge states at the chiral metal-insulator transition. These states are characterized by their specific participation ratio as a function of energy and wire width w, their distribution of coefficients in an expansion in eigenstates of the clean 2DES, and the spatial distribution of the eigenfunction amplitudes. This allows us to identify the state at the transition as a superposition of edge states of opposite chirality.

The final section contains our conclusions, and a discussion on how the CMIT could be observed experimentally.

II. THE QUANTUM PHASE DIAGRAM OF THE CMIT

Using the transfer matrix method,[13] we have calculated the two-terminal conductance[14] G as a function of energy E in a tight-binding model with bandwidth $8t$, where t is the hopping amplitude, of a disordered quantum wire in a perpendicular magnetic field (Fig. 1), with hard wall boundary conditions at $y=\pm L_{\mathrm{bulk}}/2$ and finite length $L=2000a$.[12] Here we have assumed a square lattice with lattice spacing a. The disorder potential is uniformly distributed in an interval $[-W/2, W/2]$. These results are summarized in the phase diagram (Fig. 1), where the value of G, in units of e^2/h, is given as a function of bulk width L_{bulk} and energy E in units of $\hbar\omega_B$, for a disorder strength $W=0.8t$. As expected, $G=m$, where m is the number of extended edge states between the Landau bands. Close to the middle of the Landau bands, however, the conductance plateaus collapse abruptly to $G=0$.

When the wires are so narrow that the edge states cannot form, as is the case when the width is smaller than the cyclotron length, or when edge states of opposite chirality are

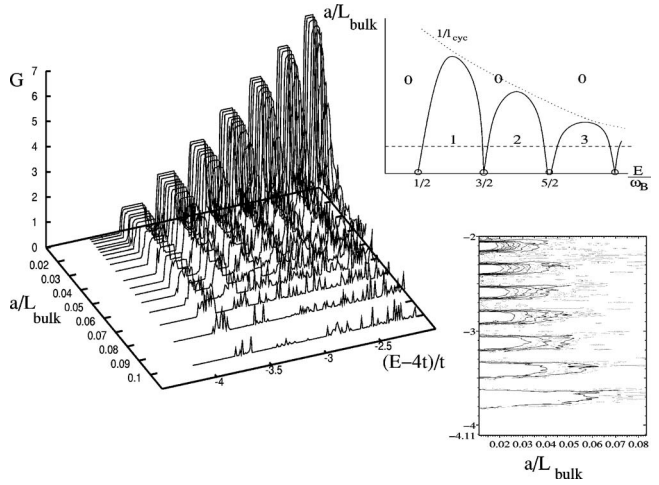

FIG. 1. The conductance as a function of energy for increasing values of the width L_{bulk} (left), and in a contour plot as a function of energy and L_{bulk} (lower right), as compared with the schematic phase diagram (upper right). Finite integer values of the conductance correspond to the number of extended edge states. The disorder is uniformly distributed in an interval of width $W=0.8t$. There are $x=0.025$ magnetic flux quanta per elementary cell of area a^2.

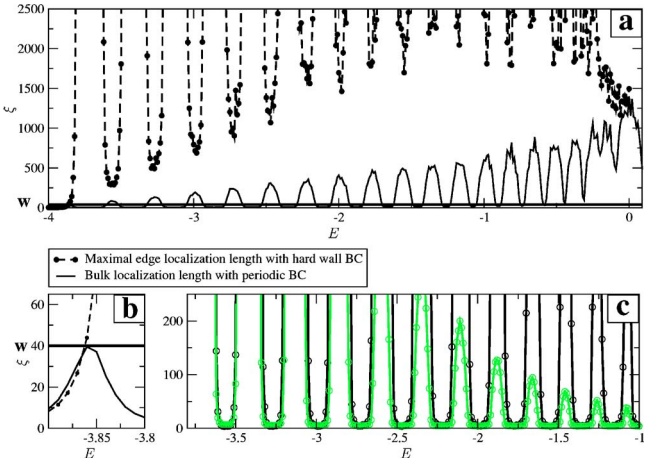

FIG. 2. (Color online) (a) The localization length for a disordered wire calculated with the transfer matrix method with periodic boundary conditions (full line) and with hard wall boundary conditions (dashed line) for uniformly distributed uncorrelated disorder in an interval of width $W=0.8t$. The straight line indicates the bulk width $w=40a$. There are $x=0.025$ magnetic flux quanta per elementary cell of area a^2. (b) Enlargement of the low-energy region of (a). Edge and bulk localization lengths coincide as long as no edge state is present. (c) The functions $\xi_{\text{edge}}/\xi(E)$ (black) and $e^{2w/\xi}$ [gray (green)].

mixed by backscattering, then all the states become localized and the conductance is vanishing with only small mesoscopic fluctuations due to the finite length L of the wire. Previously, it has been pointed out that, when the bulk localization length ξ is smaller than the physical wire width w, backscattering between edges is exponentially suppressed. As a result, the localization length of edge states increases strongly.

The overlap of opposite edge states is known to decrease exponentially with increasing wire width w.[6] Thus, the backscattering rate between edges, being proportional to the square of the overlap integral, is $1/\tau \sim \exp(-2w/\xi)$. Since the edge states are one dimensional, their localization length due to the backscattering is given by $\xi_{\text{edge}}=2v_F\tau$, with Fermi velocity v_F. On the other hand, when the bulk localization length ξ becomes equal to the wire width, one expects that the edge states become mixed with the bulk states, and localized with a length proportional to the bulk localization length ξ. Therefore, we conjectured the edge localization length to behave like[12]

$$\xi_{\text{edge}} = \xi \exp(2w/\xi). \tag{1}$$

In Fig. 2(a), the localization length is plotted as a function of energy, as obtained with the transfer matrix method in a tight-binding model of a disordered quantum wire in a perpendicular magnetic field with hard wall boundary conditions (dashed line). Since the edge states are the most extended states in the wire, this localization length can be identified with the edge localization length ξ_{edge}.

Using the transfer matrix method,[13] we have also calculated the localization length ξ as a function of energy E for a disordered quantum wire with identical properties, but with periodic boundary conditions [Fig. 2(a), solid curve]. Since there are no edge states this bulk localization length is small in the tails of Landau bands, and has maxima, which are seen to increase linearly with n.

Indeed the behavior of the edge state localization length follows qualitatively the behavior suggested by Eq. (1). The edge localization length does increase sharply, whenever the bulk localization length becomes smaller than the wire width w (full straight line). Note that the minima in the middle of the Landau bands do increase linearly with the Landau band number n. In Fig. 2(c), we have explicitly plotted ξ_{edge}/ξ and $\exp(2w/\xi)$, using the numerically calculated values for ξ_{edge} and ξ, as functions of E. We find that both functions coincide for all energies above the lowest Landau band and for $l_{\text{cyc}} < w$, so that edge states exist in the tails of the Landau bands.

An abrupt decrease of the inverse localization length has been found before for energies in the upper tail of the lowest Landau level and the tails of the second Landau level in Ref. 8. In agreement with our above results, it has been found there that the inverse localization length decays exponentially in the tails, as $1/\xi_{\text{edge}} \sim \exp[-\beta(E)w]$. The fitted values of β were found there to depend weakly on energy, whereas we identified β directly with the energy-dependent inverse bulk localization length $1/\xi(E)$.

From these results we can conclude that the energy at which edges states backscatter and become localized is given by the condition that the bulk localization length is on the order of the wire width, $\xi(E_{m,p})=w$. At this energy, m edge states mix and transitions from extended edge states to insulating states occur. This causes sharp jumps of G from finite integer to vanishingly small values, as seen in Fig. 1. This can be explained by the exponential decrease of the edge state localization length, Fig. 2. We note that $m=n$ when the energy is above the nth Landau band, whereas $m=n-1$ if it is below.

A more detailed understanding of this drastic behavior of the conductance can be obtained by considering the dimensional crossover of the bulk localization length in disordered wires.[12,15] In a 2DES with broken time reversal symmetry, scaling theory[16–19] and numerical scaling studies[13,20] find that the bulk localization length ξ is independent of the wire width, $\xi_{2D}=l_0\exp(\pi^2 g^2)$. Here, g is the 2D conductance parameter per spin channel. l_0 is the short-distance cutoff, and the elastic mean free path $l=2g(B=0)/k_F$ (k_F is the Fermi wave number) at weak magnetic fields $b\equiv\omega_B\tau<1$. For stronger magnetic fields $b>1$, the short length scale l_0 becomes the cyclotron length l_{cyc}. The conductance parameter g exhibits Shubnikov–de Haas oscillations as a function of magnetic field for $b>1$. Maxima occur when the Fermi energy is in the center of the Landau bands. The localization length in the tails of the Landau bands, where $g\ll 1$ is very small, is of the order of the cyclotron length $l_{\mathrm{cyc}}=v_F/\omega_B=\sqrt{2n+1}l_B$. It increases toward the centers of the Landau bands, $E_{n0}=\hbar\omega_B(n+1/2)$ ($n=0,1,2,\ldots$), with $\omega_B=eB/m^*$ the cyclotron frequency (e is the elementary charge and m^* the effective mass), v_F the Fermi velocity, and $l_B^2=\hbar/eB$ the magnetic length. In an *infinite* 2DES in perpendicular magnetic field, the localization length at energy E diverges as $\xi\sim|E-E_{n0}|^{-\nu}$. The critical exponent ν is known from numerical finite-size scaling studies for the lowest two Landau bands, $n=0,1$, to be $\nu=2.33\pm0.04$ for spin-split Landau levels,[21,22] in agreement with analytical[24] and experimental studies.[25] In a *finite* 2DES, a region of state exists in the centers of disorder-broadened Landau bands, which cover the whole system of size L. The width of these regions is given by $\Delta E=(l_{\mathrm{cyc}}/L)^{1/\nu}\Gamma$, where $\Gamma=\hbar(2\omega_B/\pi\tau)^{1/2}$ is the bandwidth, with elastic scattering time τ.

However, the 2D localization length is seen to increase strongly from band tails to band centers, even when the wire width w is so narrow that it is far from the critical point at $w\to\infty$. One can estimate the noncritical localization length for uncorrelated impurities, by inserting g, as obtained within self-consistent Born approximation.[23] Its maxima are $g(E=E_{n0})=(2n+1)/\pi=g_n$. Thus, $\xi_{2D}(E_{n0})=l_{\mathrm{cyc}}\exp(\pi^2 g_n^2)$ are macroscopically large in the centers of higher Landau bands, $n>1$.[22,26] When the width of the system w is smaller than ξ_{2D}, electrons in the centers of Landau bands can diffuse between the edges of the system. In long wires, however, the electrons are localized due to quantum interference along the wire with a localization length that is found to depend linearly on g and w,[12,27–29]

$$\xi_{1D}=2g(B)w. \tag{2}$$

The conductance per spin channel $g(b)=\sigma_{xx}(B)/\sigma_0$ is given by the Drude formula $g(b)=g_0/(1+b^2)$ ($g_0=E\tau/\hbar$, $b=\omega_B\tau$) for weak magnetic fields $b<1$. For $b>1$, when the cyclotron length l_{cyc} is smaller than the mean free path l, disregarding the overlap between Landau bands, g is obtained in the self-consistent Born approximation,[23] $g(B)=(1/\pi)(2n+1)[1-(E_{\mathrm{F}}-E_n)^2/\Gamma^2]$, for $|E-E_n|<\Gamma$. One obtains the localization length for $b>1$ and $|\epsilon/b-n-1/2|<1$ by inserting g. It oscillates between maximal values in the centers of Landau bands, and minimal values in the band tails. For $n>1$, one finds in the band centers

$$\xi_n=\frac{2}{\pi}(2n+1)w\left[1-\frac{\ln\sqrt{1+(w/l_{\mathrm{cyc}})^2}}{(n+1/2)^2}\right]^{1/2}. \tag{3}$$

Thus, the localization length in the center of the Landau bands is found to increase linearly with Landau band index n. This is exactly the behavior observed above in the numerical results, Fig. 2.

While it is reasonable to conclude that the edge states do mix with the bulk states at the energy where the bulk localization length is equal to the wire width, and the electrons diffuse freely from edge to edge but are localized along the wire, the question arises as to how exactly this transition from extended edge states to localized states occurs. One can gain some further insight by connecting the two ends of the wire together to form an annulus. Piercing magnetic flux through the annulus affects only states whose localization length is larger than the circumference of the annulus. The guiding centers of those states that extend around the annulus do shift in position and energy[1] with a change in magnetic flux. As shown above, in the middle of the Landau band, the electrons can diffuse freely from edge to edge, but are localized along the annulus with $\xi>w$. When the magnetic flux changes adiabatically, the energy of an edge state changes continuously. However, it cannot enter the band of localized states, so that at the energy E_m, with $\xi(E_m)=w$, the edge state must be transferred to the opposite edge. There it moves up in energy when the magnetic flux is increased further.[1]

In the following, we study the states at this transition in detail in order to find out whether the edge states become localized mainly by mixing completely with the bulk states, or rather the transition from extended chiral edge states to localized states occurs due to the nonlocal coherent superposition of edge states with opposite chirality, located at opposite edges.

III. EXACT DIAGONALIZATION

In this section, we study the localization properties of electrons in quasi-one-dimensional wires in the presence of disorder and a strong magnetic field by means of exact diagonalization.

A. The model

The Hamiltonian of the quasi-1D wire in the presence of a disorder potential V_{dis} and a confinement potential V_{conf} is given by

$$H=\frac{1}{2m^*}(\mathbf{p}-e\mathbf{A})^2+V_{\mathrm{dis}}(\mathbf{r})+V_{\mathrm{conf}}(\mathbf{r}), \tag{4}$$

where $e>0$ is the elementary charge and m^* the effective electron mass.

The disorder potential is modeled as

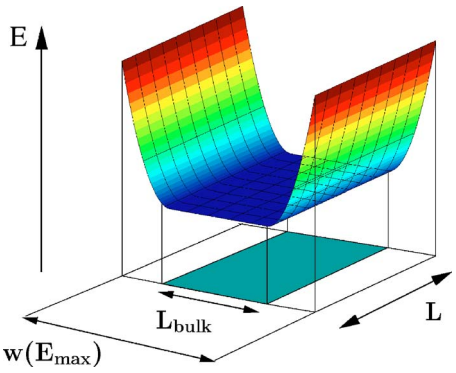

FIG. 3. (Color online) Model of a quantum wire with length L, parabolic confinement, and finite bulk region of width L_{bulk}. The physical width $w(E_{max})$ is indicated, where E_{max} is the largest energy considered.

$$V_{dis}(\mathbf{r}) = \sum_{i=1}^{N_{imp}} V_i \delta(\mathbf{r} - \mathbf{r}_i), \tag{5}$$

where N_{imp} is the number of impurities with uniformly distributed amplitude $V_i \in [-V_0, V_0]$. $\mathbf{r}_i$ is the random position of the impurity.

As we seek to investigate the interplay between and localization of edge states and bulk states in a quantum wire, we assume periodic boundary conditions in the x direction along the wire and choose

$$V_{conf}(y) = \begin{cases} \frac{1}{2}m\omega_p^2(y - L_{bulk}/2)^2, & y \geqslant L_{bulk}/2, \\ 0, & -\frac{1}{2}L_{bulk} < y < \frac{1}{2}L_{bulk}, \\ \frac{1}{2}m\omega_p^2(y + L_{bulk}/2)^2, & y \leqslant -L_{bulk}/2, \end{cases} \tag{6}$$

as confinement potential in the transversal direction (see Fig. 3). This model allows us to tune the confinement strength with the parameter ω_p. The wire width is now defined by the bulk width L_{bulk}. In the limit $L_{bulk}=L$, we get the usual 2D model for the quantum Hall effect,[30] while for $L_{bulk}=0$ we have the parabolic wire model.[31] In the limit of large confinement frequency $\omega_p > \omega_c$, one approaches hard wall boundary conditions. This type of confinement provides a smooth transition between the edge potential and the potential-free bulk region and renders the situation in real wires better than assuming hard wall boundaries.

The physical width w of parabolic wires w is a function of the Fermi energy E,

$$w(E, L_{bulk}) = 2\sqrt{\frac{2E - \hbar\Omega}{\hbar\omega_B}}\frac{\omega_B}{\omega_p} l_B + L_{bulk}, \tag{7}$$

with $\Omega = \sqrt{\omega_p^2 + \omega_B^2}$. It is obtained by finding the energy eigenvalue of the clean wire that is equal to E and has its guiding center at $\pm w/2$. We fix the basis width L_{basis} to be larger than the physical width $w(E_{max})$ at the highest considered energy E_{max}. The total number of magnetic flux quanta in the model system is then fixed to $N_\phi = L_{basis}L/(2\pi l_B^2)$.

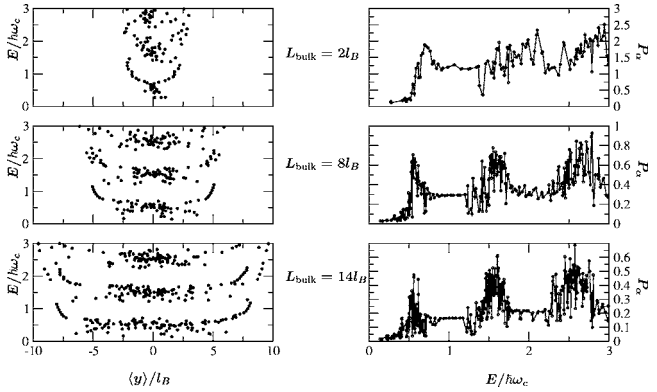

FIG. 4. Left: The energy eigenvalues E_α of all states in a wire of length $L=40.1l_B$ in a perpendicular magnetic field of 8 T for three different bulk widths are plotted versus the expectation value of the transversal position $\langle\alpha|y|\alpha\rangle$. The disorder amplitude is fixed to $V_0 = 0.73\hbar\omega_c$ with $N_i=150$ impurities and the confinement energy is chosen to have the same magnitude with $\hbar\omega_p = 0.73\hbar\omega_c$. The basis width is chosen as $L_{basis}=1.5w(E_{max})$, Eq. (7), with $E_{max}=2\hbar\omega_c$. Right: Corresponding participation ratio P_α versus E_α.

B. Wave function analysis

The Hamiltonian Eq. (4) is diagonalized in the Landau representation with basis functions

$$\langle \mathbf{r}|nX\rangle = \frac{1}{(l_B L\sqrt{\pi}2^n n!)^{1/2}} e^{-(y-X)^2/2l_B^2} H_n\left(\frac{y-X}{l_B}\right) e^{-iXx/l_B^2}. \tag{8}$$

Here we have assumed the Landau gauge for the vector potential. The matrix elements of the confinement potential in the Landau representation are given in the Appendix.

The exact diagonalization of the Hamiltonian (4) yields eigenenergies E_α with corresponding wave functions

$$\psi_\alpha(\mathbf{r}) = \sum_{nX} \langle \mathbf{r}|nX\rangle\langle nX|\alpha\rangle. \tag{9}$$

The spatial extension of these wave functions is characterized by their participation ratio

$$P_\alpha = \left(L_{bulk} L \int d^2r |\psi_\alpha(\mathbf{r})|^4\right)^{-1}, \tag{10}$$

which is small for localized states and large for extended states. Note that in this definition, P_α relates to the fixed bulk area $L_{bulk}L$ while the wave functions can cover a larger area due to the smooth confinement, so that $P_\alpha > 1$ is possible for all states.

In clean 2D systems all states in a Landau level are degenerate. In a disordered wire this degeneracy is lifted by the disorder, and at the edges by the confinement potential. Therefore, localized states in the tail of the Landau bands in the bulk region near the center of the wire coexist with states at the edges at the same energy, and, in principle, mixing of states from the bulk with edge states is possible.

These features are clearly seen in the left part of Fig. 4. For a wire of length $L=40.1l_B$ in a perpendicular magnetic field of $B=8$ T, corresponding for $m^*=0.067$ in units of the

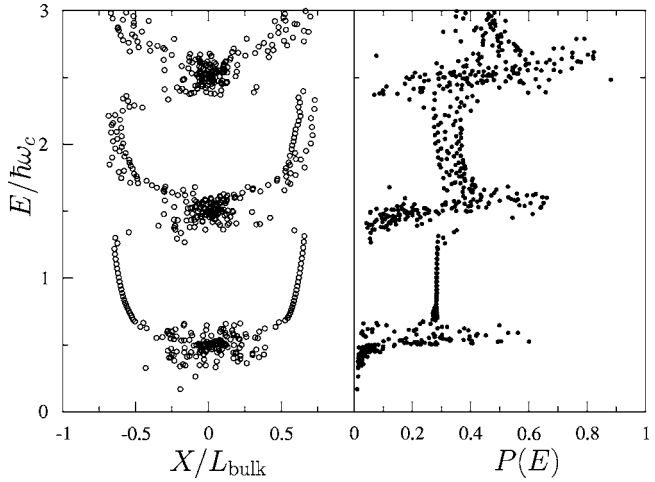

FIG. 5. Energy dispersion $E(X)$ and corresponding participation ratio $P(E)$ for a longer system with $L=100l_B$ and $L_{\mathrm{bulk}}=8l_B$ at $B=8$ T. The disorder is realized by 400 scatterers with uniformally distributed amplitude with maximal value $V_0=0.73\hbar\omega_c$ which equals the confinement energy $\hbar\omega_p=0.73\hbar\omega_c$.

bare electron mass to $\hbar\omega_c=13.82$ meV, for three different bulk widths L_{bulk} the eigenenergies are plotted versus the expectation value of their transversal position $\langle\alpha|y|\alpha\rangle$. Although we have chosen a smooth confinement potential, these results are in good agreement with earlier results with short-ranged disorder in Ref. [7]. Obviously, the edge states between the Landau bands are hardly affected by the disorder potential. There is a coupling of edge states of the same chirality in the second and higher Landau bands which leads to the formation of minibands in between the Landau band,[7] as seen most clearly in Fig. 5. There, we show the same quantities for a longer system with $L=100l_B$ and $L_{\mathrm{bulk}}=8l_B$ at $B=8$ T. The disorder is realized by 400 scatterers with $V_0=0.73\hbar\omega_c$, with the same value as the confinement energy $\hbar\omega_p=0.73\hbar\omega_c$. However, there is an abrupt shift of the center of the eigenstates toward the middle of the wire, when their energy is approaching the middle of the Landau band. Still, one cannot conclude whether this fact is mainly due to the backscattering between edge states from opposite edges having opposite chirality, or whether it is mainly due to a mixing with the bulk localized states.

In order to learn more about the nature of these states, we have calculated the Fermi energy dependence of the participation ratio for different bulk widths with fixed disorder potential and constant magnetic field as shown in the right part of Figs. 4 and 5. It is observed for all three widths that the participation ratio and the eigenenergies fluctuate as a result of disorder especially in the center of the wire. The participation ratio increases with energy in the tails of the Landau bands and reaches a maximum close to the corresponding center energy [between $0.5\hbar\omega_c$ for $L_{\mathrm{bulk}}\to\infty$ and $0.5\hbar(\omega_c^2+\omega_p^2)^{1/2}$ for $L_{\mathrm{bulk}}\to 0$]. The participation ratio saturates to a constant value between the Landau bands, where only edges states exist, as confirmed by comparison with the left side of Fig. 4.

In the following, we scrutinize the localization behavior in the different energy regions identified above by the energy

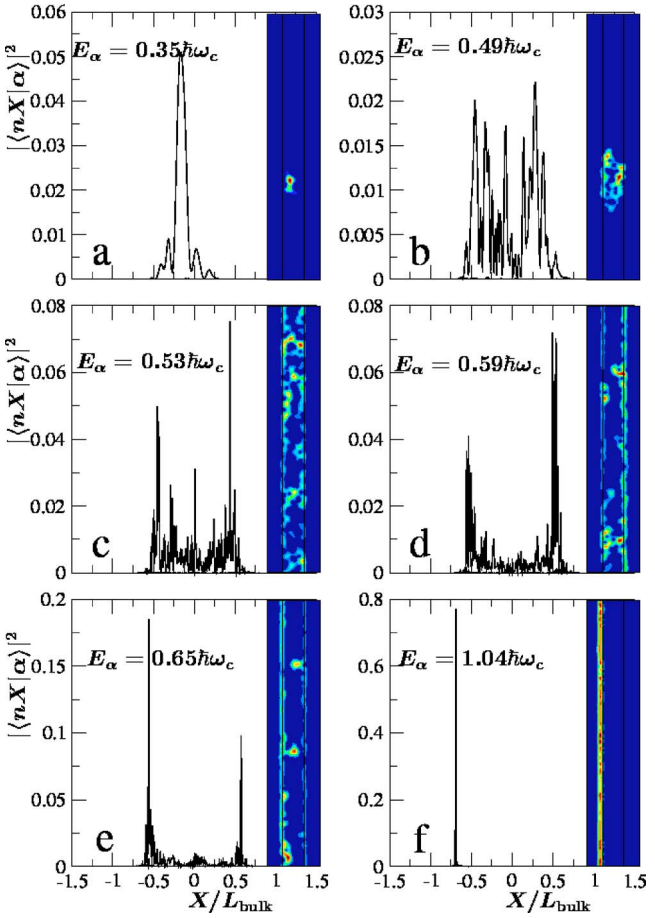

FIG. 6. (Color online) Basis state contributions to eigenstates at selected energies. The right insets show the corresponding probability densities [blue (dark) for low, red (bright) for high values], solid lines mark the bulk region. System parameters are the same as in Fig. 5.

dispersion and the participation ratio. To determine the nature of the states, we plot the basis state contributions and spatially resolved probabilities for a sample with $L=100l_B$ and $L_{\mathrm{bulk}}=8l_B$ at typical energies, with disorder amplitude and confinement energy comparable to the cyclotron energy. We concentrate on the lowest Landau level and investigate wave functions at energies in characteristic regions of the participation ratio. The result is displayed in Fig. 6.

We find states at $E=0.3\hbar\omega_c$ [Fig. 6(a)] which are 2D localized, as confirmed by the fact that they have contributions from basis states with guiding centers in the bulk region only. In the band center around $E=0.5\hbar\omega_c$ the participation ratio fluctuates strongly. In this region we find 2D localized states as well as 1D localized states with a localization length larger than the bulk width, but much smaller than the wire length [Fig. 6(b)]. In the latter case, basis states from bulk and edge regions mix with comparable contributions. Furthermore, we can identify states that cover the whole sample, as shown in Fig. 6(c). These states couple to all regions as well, although the contributions from the left and right edges seem to prevail slightly. The trend indicated by the maxima close to the edges intensifies in the transition region [Fig. 6(d)]. At a specific energy, the contribution of the bulk states

is small compared to the sharp maxima at the edges, while the electron is found with the same probability on the right *or* the left edge of the wire [Fig. 6(e)]. We believe that this nonchiral edge state is unique at least in the thermodynamic limit of $w \to \infty$ and governs the chiral metal-insulator transition in quasi-1D quantum Hall wires. This state exhibits notable localization features: being an edge state concerning the participation ratio, it has to be considered localized concerning the conductance, since current flows with equal probability but reversed sign on both edges. This behavior is consistent with the sudden breakdown of the conductance observed in Fig. 1.

At higher energies, below the next Landau band, edge states are formed as seen in Fig. 6. These states are found to be insensitive to disorder.

This sequence of transitions from 2D bulk states, quasi-1D localized states, states with peaks on both edges of the wire, and decoupled edge states is visible in Fig. 7(a), where we show the basis state contributions for every fifth state in the lowest Landau level. All features discussed above are seen clearly, with a remarkably narrow transition region from 1D localized states to edge states, as one moves from state 125 to state 145.

In order to visualize this transition in detail, we plot in this interval all states in Fig. 7(b). The higher-energy states are clearly edge states, which are decoupled from the bulk, and are altenatingly located either on the left or on the right side of the wire. The lower the energy, the smaller becomes that peak in intensity at the edge. Still, each state stays located in the edge region, with only a small coupling to the nearest part of the bulk. Then, suddenly, at state (α=143 in Fig. 7), there appear two peaks of comparable amplitude on both edges, while the contribution of the bulk is still small. All states α=139–143 share the two pronounced peaks at the edges, while the bulk contribution increaes only slowly with lowering energy. Before the transition to quasi-1D states with more or less uniform distribution across the bulk, there is a reappearance of edgelike states α=135–138, which we attribute to mesoscopic fluctuations due to the random distribution of disorder in this rather mesoscopic sample. The transition that we observed here thus happens rather smoothly as compared to the sharp transitions in the transfer matrix results shown in Fig. 1. This can be attributed to the fact that the finite system with $L=100l_B$ that we have diagonalized here is much smaller than the system that was handled by the transfer matrix method. As expected far away from the thermodynamic limit, $L, w \to \infty, L/w$=const, the transition occurs in a finite energy interval rather than at a single point. Finite-size effects can be revealed further by studying the dependence of the states on the bulk width.

To this end we next study the system size dependence of the participation ratio. Figure 8 shows the participation ratio of all states in a given energy interval for systems with different bulk widths L_{bulk}. Disorder configuration, wire length, and confinement energy $\hbar\omega_p$ are kept fixed for all the systems. As a characteristic example for the behavior in the low-energy region, we investigate states in an interval around energy $E=0.2\hbar\omega_c$ [Fig. 8(a)]. In this region, the participation ratio scales with the wire width approximately as $P \propto L_{\text{bulk}}^{-1}$. This is in agreement with the expected scaling of

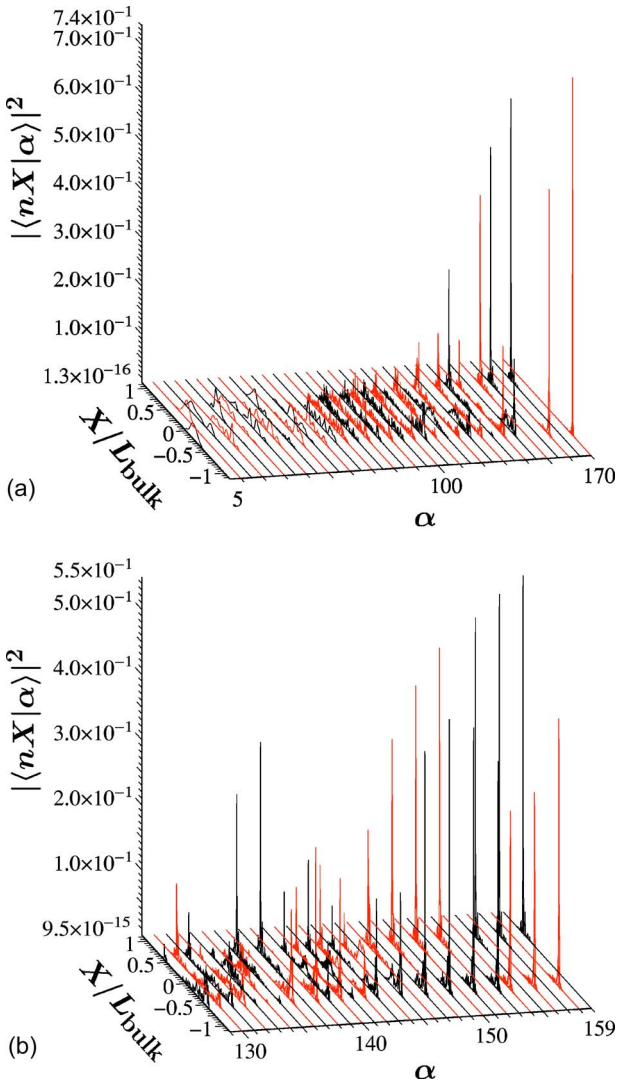

FIG. 7. (Color online) Basis state contributions $|\langle nX|\alpha\rangle|^2$ to eigenstates α at different energies (a) for every fifth state in the lowest Landau level and (b) for every state with energy between $0.6\hbar\omega_c$ and $0.8\hbar\omega_c$. System parameters are the same as in Fig. 5. Different shades are used for adjacent curves in order to distinguish them clearly.

2D localized states, which give a contribution $\psi_\alpha^2 \propto 1/\xi_{2\text{D}}^2$ only within a localization area $\xi_{2\text{D}}^2$ where $\xi_{2\text{D}}$ is the 2D localization length of the wave function, which is independent of the wire length L and width L_{bulk}. It follows that

$$P_{2\text{D}} \propto \xi_{2\text{D}}^2 L^{-1} L_{\text{bulk}}^{-1} \ll 1, \tag{11}$$

in good agreement with Fig. 8(a).

The behavior changes in the center of the Landau band [Fig. 8(b)]. There, the density of states is higher, and the disorder results in a wide range of participation ratios. For large bulk widths $L_{\text{bulk}} > 5l_B$, the range of participation ratios becomes constant and saturates to a finite value. Note that quasi-1D localized states cover approximately an area $L_{\text{bulk}}\xi_{1\text{D}} \sim gL_{\text{bulk}}^2$, and contribute in this area with probability density $\psi_\alpha^2 \sim 1/(\xi_{1\text{D}}L_{\text{bulk}})$. As a result, one expects for quasi-1D localized states, according to Eq. (2),

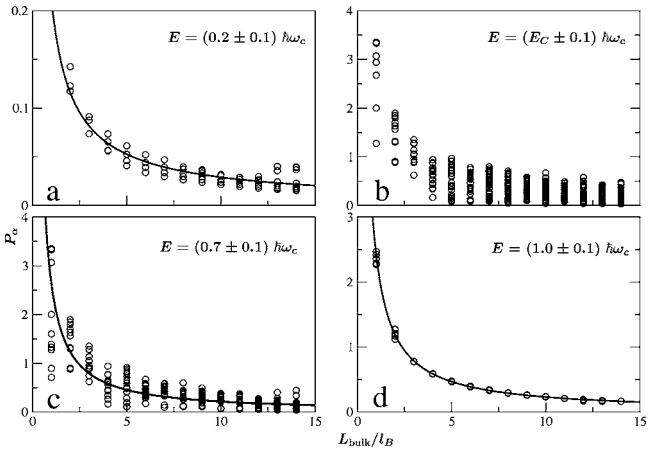

FIG. 8. Participation ratio in dependence on bulk width for different energies. E_C is determined for each bulk width as the energy at which the system reaches the maximal participation ratio in the lowest Landau band. System parameters are the same as in Fig. 4. Solid lines are fitting functions: (a) $P_\alpha=0.21\ (L_{\rm bulk}/l_B)^{-0.86}$, (c) $P_\alpha=2.62\ (L_{\rm bulk}/l_B)^{-1.09}$, and (d) $P_\alpha=2.41\ (L_{\rm bulk}/l_B)^{-1.02}$.

$$P_{\rm 1D} \propto \frac{\xi_{\rm 1D}}{L} \sim g\frac{L_{\rm bulk}}{L}, \tag{12}$$

increasing linearly with $L_{\rm bulk}$. When the wire is comparable to or shorter than the quasi-1D localization length, however, the participation rato shows rather the behavior of 2D extended states which cover the whole wire area Lw with probability density $1/(Lw)$, yielding the typical participation rato of extended states

$$P_{\rm ext} \sim w/L_{\rm bulk} = {\rm const} > 1, \tag{13}$$

independent of the width $L_{\rm bulk}$. Note that for extended states one would expect $P_\alpha=w/L_{\rm bulk}$, which according to Eq. (7) converges to 1 for $L_{\rm bulk}\to\infty$. Whereas P_α in Fig. 8(b) is indeed seen to saturate to a constant mean value, this value is found not to exceed 1. This is consistent with the fact that the wave function is multifractal.[34]

The scaling of the participation ratios in the high-energy tail of the lowest Landau band [Figs. 8(c) and 8(d)] is again a power law $P\propto L_{\rm bulk}^{-1}$, but with an absolute value much larger than in Fig. 8(a). This resembles the expected feature for edge states, which cover an area l_BL with probability density $1/(l_BL)$, yielding

$$P_{\rm edge} \propto l_B/L_{\rm bulk}, \tag{14}$$

which is both in magnitude and in the functional dependence on $L_{\rm bulk}$ in good agreement with Fig. 8(d). Note that in the transition region, Fig. 8(c), the large mesoscopic fluctuations do not allow one to distinguish characteristic features of the nonchiral edge states at the transition; the functional dependence on $L_{\rm bulk}$ is that expected for edge states and localized bulk states alike, which both coexist in this energy region, as we saw above in Fig. 7.

In summary, our model allows us to study the mutual influence between the states in the bulk region, where the influence of the disorder potential is strong, and states in the edge region, where the confinement potential prevails. We found that in the narrow energy region of the CMIT the disorder-induced coupling between the edges creates nonchiral edge states which have comparable weights on both edges, but only a negligible mixing with the bulk.

IV. CONCLUSIONS

We conclude that in quantum Hall bars of finite width $w \ll \xi_n$ at low temperatures quantum phase transitions occur between extended chiral edge states and a quasi-1D insulator. These are driven by the crossover from 2D to 1D localization of bulk states. These metal-insulator transitions resemble first-order phase transitions in the sense that the localization length abruptly jumps between exponentially large and finite values, which we confirmed by calculating the edge state localization length explicitly. In the thermodynamic limit, fixing the aspect ratio $c=L/w$, when sending $L\to\infty$ and then $c\to\infty$, the two-terminal conductance jumps between exactly integer values and zero. The transitions occur at energies where the localization length of bulk states is equal to the geometrical wire width. Then, m edge states mix and electrons are free to diffuse between the wire boundaries but become Anderson localized along the wire. Close to that transition we found with exact diagonalization studies that particular states exist which are superpositions of edge states with opposite chirality, with an order of magnitude smaller bulk contribution. Although these states are located at the edges, they are nonlocal states, having comparable weights on opposite sides of the sample. Thus, it can have a mesoscopic extension across the width of the Hall bar, if it is narrower than the phase coherence length. The chiral metal-insulator transition is of mesoscopic nature since, at finite temperature, the phenomenon of the CMIT can only be observed when the phase coherence length exceeds the quasi-1D localization length in the centers of Landau bands, $L_\varphi > \xi_n$. One then should observe transitions of the two-terminal resistance from integer quantized plateaus $R_n = h/ne^2$ to a Mott variable-range hopping regime of exponentially diverging resistance. Such experiments would yield information about the coupling between edge and bulk states in quantum Hall bars. At higher temperature, when $L_\varphi < \xi_n$, the conventional form of the integer quantum Hall effect is recovered.[32,33]

We have studied the modification of the CMIT by correlations in the disorder potential and due to interactions. These results will be presented in a subsequent publication.

ACKNOWLEDGMENTS

We acknowledge useful discussions with M. E. Raikh, A. MacKinnon, and B. Huckestein. This research was supported by German Research Council (DFG), Grant No. Kr 627/10, Schwerpunkt "Quanten-Hall-Effekt," and by EU TMR network Grant. No. HPRN-CT2000-0144.

APPENDIX: MATRIX ELEMENTS FOR CONFINEMENT IN LANDAU REPRESENTATION

The matrix element of the confinement potential defined by Eq. (6) in Landau representation $\langle nX|V_{\rm conf}|n'X'\rangle$ is given by

$$\langle nX|V_{\text{conf}}|n'X'\rangle = \delta_{XX'}\frac{1}{\sqrt{\pi}l_B 2^{(n+n')}n!n'!}\left[M_{nn'}\left(\frac{L_{\text{bulk}}}{2},X\right) + (-1)^{(n+n')}M_{nn'}\left(\frac{L_{\text{bulk}}}{2},-X\right)\right] \tag{A1}$$

and

$$M_{nn'}\left(\frac{L_{\text{bulk}}}{2},X\right) = \int_{L_{\text{bulk}}/2}^{\infty} dy\, e^{-(y-X)^2/l_B^2}H_n\left(\frac{y-X}{l_B}\right) \times H_{n'}\left(\frac{y-X}{l_B}\right)\left(\frac{y-L_{\text{bulk}}/2}{l_B}\right)^2 \tag{A2}$$

$$= l_B\int_b^{\infty} d\xi\, e^{-\xi^2}(\xi-b)^2H_n(\xi)H_{n'}(\xi), \tag{A3}$$

where $\xi=(y-X)/l_B$ and $b=(L_{\text{bulk}}/2-X)/l_B$.

By expanding all polynomials in Eq. (A3) in monomials in ξ using the relation

$$H_n(\xi) = n!\sum_{m=0}^{[n/2]}(-1)^m\frac{2^{n-2m}}{m!(n-2m)!}\xi^{n-2m}, \tag{A4}$$

where $[x]$ denotes the largest integer smaller than x, one gets

$$M_{nn'}(b,X) = l_B n!n'!\sum_{l=0}^{[n/2]}\sum_{k=0}^{[n'/2]}\left[(-1)^{l+k}\frac{2^{n-2l+n'-2k}}{l!k!(n-2l)!(n'-2k)!} \times [f^{(2+n-2l+n'-2k)}(b) - 2bf^{(1+n-2l+n'-2k)}(b) + b^2f^{(n-2l+n'-2k)}(b)]\right].$$

In the last expression,

$$f^{(M)}(b) = \int_b^{\infty} d\xi\, \xi^M e^{-\xi^2} = \frac{M-1}{2}f^{(M-2)}(b) + b^{M-1}\frac{1}{2}e^{-b^2}. \tag{A5}$$

This recursive formula can be obtained by repeated partial integration and is valid for even and odd $M>1$. An explicit evaluation requires the inital expressions

$$f^{(0)}(b) = \frac{1}{2}e^{-b^2}, \tag{A6}$$

$$f^{(1)}(b) = \frac{1}{2}\sqrt{\pi}\,\text{erfc}(b), \tag{A7}$$

with the complementary error function

$$\text{erfc}(b) = \int_b^{\infty} d\xi\, e^{-\xi^2}. \tag{A8}$$

[1] B. I. Halperin, Phys. Rev. B **25**, 2185 (1982).
[2] R. J. Haug and K. von Klitzing, Europhys. Lett. **10**, 489 (1989).
[3] G. Timp *et al.*, Phys. Rev. Lett. **59**, 732 (1987); G. Timp, R. Behringer, T. E. Cunningham, and R. E. Howard, *ibid.* **63**, 2268 (1989); E. Peled, D. Shahar, Y. Chen, D. L. Sivco, and A. Y. Cho, *ibid.* **90**, 246802 (2003).
[4] T. Ando, Phys. Rev. B **49**, 4679 (1994).
[5] B. J. van Wees *et al.*, Phys. Rev. B **43**, 12431 (1991).
[6] B. I. Shklovskii, Pis'ma Zh. Eksp. Teor. Fiz. **36**, 43 (1982) [JETP Lett. **36**, 51 (1982)]; A. V. Khaetskii and B. I. Shklovskii, Zh. Eksp. Teor. Fiz. **85**, 721 (1983) [Sov. Phys. JETP **58**, 421 (1983)]; M. E. Raikh and T. V. Shahbazyan, Phys. Rev. B **51**, 9682 (1995).
[7] T. Ohtsuki and Y. Ono, Solid State Commun. **65**, 403 (1988); **68**, 787 (1988); Y. Ono, T. Ohtsuki, and B. Kramer, J. Phys. Soc. Jpn. **58**, 1705 (1989); T. Ohtsuki and Y. Ono, *ibid.* **58**, 956 (1989).
[8] T. Ando, Phys. Rev. B **42**, 5626 (1990).
[9] R. G. Mani and K. v. Klitzing, Phys. Rev. B **46**, R9877 (1992); R. G. Mani, K. von Klitzing, and K. Ploog, *ibid.* **51**, 2584 (1995).
[10] P. G. N. deVegvar *et al.*, Phys. Rev. B **36**, R9366 (1987).
[11] M. L. Roukes *et al.*, Phys. Rev. Lett. **59**, 3011 (1987).
[12] S. Kettemann, B. Kramer, and T. Ohtsuki, JETP Lett. **80**, 316 (2004).
[13] B. Kramer and A. MacKinnon, Rep. Prog. Phys. **56**, 1469 (1993).
[14] J. B. Pendry, A. MacKinnon, and P. J. Roberts, Proc. R. Soc. London, Ser. A **437**, 67 (1992).
[15] S. Kettemann, J. Phys. Soc. Jpn. **72**, 197 (2003); S. Kettemann, Phys. Rev. B **69**, 035339 (2004).
[16] E. Abrahams *et al.*, Phys. Rev. Lett. **42**, 673 (1979).
[17] F. Wegner, Z. Phys. B **36**, l209 (1979); Nucl. Phys. B **316**, 663 (1989).
[18] S. Hikami, Prog. Theor. Phys. **64**, 1466 (1980).
[19] K. B. Efetov, A. I. Larkin, and D. E. Khmel'nitskii, Zh. Eksp. Teor. Fiz. **79**, 1120 (1980) [Sov. Phys. JETP **52**, 568 (1980)].
[20] A. MacKinnon and B. Kramer, Phys. Rev. Lett. **47**, 1546 (1981); Z. Phys. B: Condens. Matter **53**, 1 (1983).
[21] J. T. Chalker and G. J. Daniell, Phys. Rev. Lett. **61**, 593 (1988); B. Huckestein and B. Kramer, *ibid.* **64**, 1437 (1990).
[22] B. Huckestein, Rev. Mod. Phys. **67**, 357 (1995).
[23] T. Ando and Y. Uemura, J. Phys. Soc. Jpn. **36**, 959 (1974); **36**, 1521 (1974); **37**, 622 (1974).
[24] A. G. Galstyan and M. E. Raikh, Phys. Rev. B **56**, 1422 (1997); D. P. Arovas, M. Janssen, and B. Shapiro, *ibid.* **56**, 4751 (1997).
[25] H. P. Wei *et al.*, Phys. Rev. Lett. **61**, 1294 (1988); S. Koch *et al.*, *ibid.* **67**, 883 (1991); L. W. Engel *et al.*, *ibid.* **71**, 2638 (1993); M. Furlan, Phys. Rev. B **57**, 14818 (1998); F. Hohls *et al.*, Phys. Rev. Lett. **88**, 036802 (2002).
[26] B. Huckestein, Phys. Rev. Lett. **84**, 3141 (2000).
[27] K. B. Efetov, *Supersymmetry in Disorder and Chaos* (Cambridge University Press, Cambridge, U.K., 1997).
[28] K. B. Efetov and A. I. Larkin, Zh. Eksp. Teor. Fiz. **85**, 764 (1983) [Sov. Phys. JETP **58**, 444 (1983)].
[29] O. N. Dorokhov, Pis'ma Zh. Eksp. Teor. Fiz. **36**, 259 (1982)

[JETP Lett. **36**, 318 (1983)]; Zh. Eksp. Teor. Fiz. **85**, 1040 (1983) [Sov. Phys. JETP **58**, 606 (1983)]; Solid State Commun. **51**, 381 (1984).

[30] T. Ando, J. Phys. Soc. Jpn. **53**, 3126 (1984).

[31] M. Janßen, O. Viehweger, U. Fastenrath, and J. Hajdu, *Introduction to the Theory of the Integer Quantum Hall Effect* (VCH-Verlagsgruppe, Weinheim, 1994).

[32] K. Takashima *et al.*, Physica E (Amsterdam) **20**, 160 (2003).

[33] K. v. Klitzing, G. Dorda, and M. Pepper, Phys. Rev. Lett. **45**, 494 (1980).

[34] W. Pook and M. Janssen, Z. Phys. B: Condens. Matter **82**, 295 (1991); B. Huckestein, B. Kramer, and L. Schweitzer, Surf. Sci. **263**, 125 (1993); B. Huckestein and R. Klesse, Phys. Rev. B **55**, R7303 (1997).